## 1.6 Hydraulic Jumps, Bores, Rarefaction Waves, and Long's Experiment.

One of the traditional difficulties in learning about hydraulics is to reach an understanding of why controlled (subcritical-to-supercritical) solutions arise and how they are established. Calculations of steady flows merely show the existence of hydraulically controlled solutions for special values of the governing parameters (e.g. $\tilde{B}$ =2.5 in Figure 1.4.3) and this gives the impression that such a state might be difficult to realize in nature. On the other hand, observations and laboratory experiments show that controlled solutions prevail when topography is sufficiently high. It is valuable to observe how steady flows are established as the result of time-dependent adjustment from a simple initial state, or as the result of varying the upstream conditions. A classical example is the experiments of Long (1953,1954,1972), who towed and obstacle through a laboratory tank containing a fluid initially at rest. The initial fluid depth $d_o$ is constant and the obstacle is towed at a fixed speed $v_0$ until a translating steady state is achieved in the vicinity. For a frictionless system, the experiment is equivalent to the sudden introduction of an obstacle into a moving stream of depth and velocity $d_0$ and $v_0$ (Figure 1.6.1). This is the viewpoint we will use. The outcome depends crucially on the height $h_m$ of the obstacle relative to a threshold value $h_c$. A variety of experiments have confirmed that $h_c$ is simply the obstacle height associated with a hydraulically controlled *steady* state whose upstream depth and velocity are $d_o$ and $v_o$. This is exactly the height that appears in (1.4.11) if $Q/w$ is interpreted as $v_0 d_0$. A nondimensional form of this relation is

$$\frac{h_c}{d_0} = 1 - \frac{3}{2} F_0^{2/3} + \frac{F_0^2}{2} \qquad (1.6.1)$$

where $F_0 = \dfrac{v_0}{(g d_0)^{1/2}}$.

For $h_m < h_c$ the sudden appearance of the obstacle generates disturbances that propagate away from the obstacle and leave behind an uncontrolled steady solution, either completely supercritical or completely subcritical. When the initial state is subcritical $v_0 < (g d_o)^{1/2}$, a subcritical steady state with a dip in the upper surface is established (Figure 1.6.1b). Note that the disturbances propagating away from the obstacle are *isolated* in the sense that they do not permanently alter the flow into which they propagate. For supercritical initial flow and $h_m < h_c$, a supercritical steady state is established, this time with the two isolated disturbances propagating downstream.

When $h_m > h_c$, the situation is quite different. The obstacle now generates an upstream *bore*: a propagating wave consisting of an abrupt increase in depth. As shown in Figure 1.6.1c, the upstream bore increases the depth from $d_0$ to $d_1$. In practice, the bore can vary from a nearly discontinuous, turbulent transition to a gradual, and perhaps oscillatory, change. The latter is called an *undular bore*. Here, the bore is represented as a simple depth discontinuity. Downstream of the obstacle, the adjustment is caused by a

bore and a rarefaction wave. In some cases the downstream bore may become stationary on the down-slope of the obstacle forming a hydraulic jump (Figure 1.6.1c). Over the obstacle a hydraulically controlled steady state develops. The final steady state thus has subcritical flow upstream, supercritical flow downstream (perhaps terminating in a hydraulic jump) and critical flow at the sill. There also exists a second threshold height $h_b$ ($>h_c$) that, when exceeded, results in complete blockage of the flow (Figure 1.6.1d).

Long's experiments give a particular view of the concept of hydraulic control, one in which obstacle gains the ability to permanently alter the far field flow. When $h_m<h_c$ the long-term influence of the obstacle is local; when $h_m>h_c$ this influence is global. In the latter case, it is often said that the obstacle exerts *upstream influence (*even though the downstream flow is also altered). Another virtue of Long's experiment is that the final steady state can be predicted from the initial conditions. To do so, one must analyze the time-dependent flow that has developed long after the obstacle is introduced. In particular, sufficient time must have elapsed to allow the transients to move away from the obstacle and developed into bores and/or rarefaction waves. The analysis makes use of *shock-joining* conditions linking the uniform flows on either side of the transients. The full solution to the adjustment problem will be presented in the next section; first we must develop a theory for shock joining.

*a. Shock joining.*

Bores and hydraulic jumps are nonhydrostatic and often highly turbulent. Both produce changes in the thickness and velocity that take place over a distance of the order of the fluid depth. This distance is very short in the context of our long-wave model and can formally be treated as a discontinuity in $d$ and $v$. Away from the discontinuity the pressure is hydrostatic and the velocity independent of depth. As an example, consider a hydraulic jump consisting of a stationary discontinuity between two steady flows (Figure 1.6.2). Let $(d_u,v_u)$ and $(d_d,v_d)$ denote the depth and velocity immediately upstream and downstream of the jump. In practice, one must measure these end-state values far enough away from the jump that the fluid is hydrostatic. Then it is immediately clear from mass conservation that

$$v_u d_u = v_d d_d. \qquad (1.6.2)$$

Although the channel width $w$ may vary with $y$, the assumed abrupt nature of the jump means that the gradually varying $w$ is essentially the same on each side of the jump. Hence $w$ does not enter the above mass balance.

A second matching condition can be obtained from the observation that no external forces in the $y$-direction act on the fluid at the discontinuity. In practice, there might be a frictional stress acting along the bottom or a pressure component in the $y$-direction resulting from a non-zero bottom slope; however, the force arising from this stress will be negligible if the length of the shock is sufficiently short. Hence the difference in the pressure forces on either side of the jump must equal the change in the momentum flux of fluid entering and leaving the jump. The total pressure force acting over a section of the flow is the integral of the hydrostatic pressure $p$ over that section,

$\rho w g d^2/2$. The total momentum flux across the section is $\rho w v^2 d$. Our momentum budget therefore requires

$$d_u v_u^2 + g d_u^2/2 = d_d v_d^2 + g d_d^2/2\,, \tag{1.6.3}$$

The value of $w$ has again been considered equal on either side of the jump. The quantity $\rho w(d\,v^2 + g d^2/2)$ is sometimes called the *flow force* and (1.6.3) shows that it is conserved across a jump.

If the discontinuity translates steadily at speed $c_1$, the above analysis can be repeated in a frame of reference moving with the discontinuity. Since the flow appears steady in this frame, and since the governing equations are invariant with respect to steady translation, (1.6.2) and (1.6.3) are again obtained, but with $v_d$ and $v_u$ interpreted as moving frame velocities. To return to the rest frame, replace these velocities by $v_d$-$c_1$ and $v_u$-$c_1$, where $v_d$ and $v_u$ now denote the rest-frame velocities. The general shock joining relations are therefore given by:

$$(v_u - c_1)d_u = (v_d - c_1)d_d \tag{1.6.4}$$

and

$$d_u(v_u - c_1)^2 + g d_u^2/2 = d_d(v_d - c_1)^2 + g d_d^2/2 \tag{1.6.5}$$

If the end states are unsteady, the shock speed will vary with time. In this case it is possible to show that (1.6.4) and (1.6.5) continue to hold, but we leave the proof as an exercise for the reader.

Equations (1.6.2) and (1.6.3) allow the downstream state of a hydraulic jump to be calculated given a known upstream depth and velocity. These relations also show that the energy of the fluid crossing the jump is not conserved. Since $B_u = \frac{v_u^2}{2} + g d_u$ is the energy per unit mass of any fluid element entering the jump, the total energy influx is $QB_u$ and the total outflux is $QB_d$. The difference between these two is proportional to the rate of energy dissipation $-\dot{E}$ (per unit mass) within the jump. Using (1.6.2) and (1.6.3) it can be shown that

$$-\dot{E} = \frac{gQ}{4}\frac{(d_d - d_u)^3}{d_d d_u} \tag{1.6.6}$$

For a bore, the above expression is valid if $Q$ is interpreted as $(v_u - c_1)d_u w$, the transport seen in the moving frame of the bore. In either case, energy dissipation ($-\dot{E} > 0$) for positive $Q$ requires that ($d_d$-$d_u$) also be positive. More generally, energy dissipation

requires that the depth of fluid increase as the fluid passes through the jump or bore. It is remarkable that the rate of dissipation can be calculated independently of viscosity or even the form of internal dissipation.

Since a bore or jump contains no internal sources of energy, the fluid depth must increase in the direction of the flow passing through. This is an important constraint as (1.6.4) and (1.6.5) admit solutions with positive *and* negative dissipation. An example can be found through elimination of $c_1$-$v_d$ from (1.6.4) and (1.6.5), yielding

$$\left(c_1 - v_u\right)^2 = g d_d \left(\frac{d_d + d_u}{2 d_u}\right). \qquad (1.6.7)$$

The left-hand side of this relation is the speed of a bore relative to the velocity of the fluid to the left. For given $v_u$, $d_d$ and $d_u$, two solutions for $c_1$ can be found corresponding to the positive and negative square roots of the right-hand side. The positive root corresponds to fluid entering the bore from the right while the negative root corresponds to fluid entering from the left. If $d_d > d_u$ the negative root must be selected.

Returning temporarily to the case of a stationary jump, a bit of manipulation of (1.6.2) and (1.6.3) leads to

$$\frac{d_d}{d_u} = \frac{-1 + \sqrt{1 + 8 F_u^2}}{2} \qquad (1.6.8)$$

where $F_u = v_u / \sqrt{g d_u}$, the Froude number of the approach flow. Since the fluid depth must increase in the direction of the flow, $d_d/d_u > 1$ and thus $F_u$ must exceed unity. The approach flow must be supercritical. Since the subscripts *u* and *d* can be interchanged without affecting (1.6.2) and (1.6.3), an expression involving the downstream Froude number $F_d = v_d / \sqrt{g d_d}$ can be obtained simply by interchanging the subscripts in (1.6.8). Thus

$$\frac{d_u}{d_d} = \frac{-1 + \sqrt{1 + 8 F_d^2}}{2}, \qquad (1.6.9)$$

showing that the downstream flow must be subcritical. For a flow with positive *v*, waves with speeds $v$-$(gd)^{1/2}$ must move towards the jump from both upstream and downstream. A similar interpretation is possible for a bore, which overtakes linear waves propagating against the upstream flow but is overtaken from the rear by the same type of linear waves. The convergence of waves at the discontinuity is closely related to the nonlinear steepening process discussed in Section 1.3 and is instrumental in maintaining the bore. The same mechanism is related to the shock-forming instability depicted in Figure 1.4.4.

The hydraulic jump provides a mechanism by which a supercritical flow can join to a downstream subcritical flow with the same $Q$ but lower $B$. For the steady solutions sketched in Figure 1.4.3, this means that the hydraulically controlled flow ($\tilde{B}$=5/2) could

connect to one of the solutions for which $\tilde{B}<5/2$. The connection would occur in the form of a hydraulic jump on the down-slope of the obstacle, and one possibility is indicated in the figure.

The above analysis takes for granted that the jump or bore occurs over a horizontal distance short enough that bottom friction and other external sources or sinks of momentum are insignificant. For hydraulic jumps this assumption is valid as long as the Froude number of the approach flow is greater than about 1.7 (Chow, 1965). Then the depth change occurs over a horizontal distance on the order of the fluid depth. Such a change is tantamount to a discontinuity in the gradually varying framework of shallow-water dynamics. For Froude numbers <1.7 however, the jump becomes undular (wavelike) and the depth changes occur over a much longer distance. Non-hydrostatic effects are essential to the wavy structure of the jump and the increased horizontal length may necessitate consideration of additional sources of momentum. The reader is referred to Baines (1995) for a deeper discussion.

Some of the best places to observe bores are over gently sloping beaches such as those of southern California (Figure 1.6.3). On the left-hand side of the photo is a turbulent bore caused by the shallow surge of a wave running towards the beach. The middle of the photo shows a fairly quiescent, V-shaped region in which the water depth is just a few inches. To the right is the smooth, wavy front of a surge that is running away from the beach (right-to-left). The latter was generated by a previous wave that ran up on the beach and is now spilling back. This reverse surge is a good example of an undular bore.

*b. Discontinuities and matching conditions.*

Discontinuities, real or contrived, are encountered quite often in fluid dynamics. In many situations, matching conditions are found through integration across the discontinuity of the equations governing the flow away from it. Of course, this procedure is only valid when the governing equations hold at the discontinuity as well. One must take great care in applying this method to free-surface jumps and bores, for which the shallow water equations do not hold. For example, (1.6.5) cannot be derived by integrating the shallow water momentum equation (1.2.1) across the discontinuity. Doing so would lead to the incorrect conclusion that the Bernoulli function $B$ is conserved across the shock.

The safest approach in such cases is to formulate property budgets for a fixed control volume surrounding the shock. This is essentially the approach used to derive (1.6.3). An alternative, but equally valid, form of the momentum budget

$$\frac{d}{dt}\iiint_V \rho v \, dxdydz = \sum_{\partial V} F^{(y)} . \qquad (1.6.10)$$

is valid if a material control volume $V$ is used. The right-hand side is the sum of forces $F^{(y)}$ in the $y$-direction around the bounding surface $\partial V$. [The derivation of (1.6.3) using (1.6.10) is described in Exercise 2.]

A useful alternative form of the shallow water momentum equation can be derived from (1.6.10) if it is temporarily assumed that the flow fields are smooth. If $V$ is made infinitesimal and the shallow water approximations are applied, the result is the so called *flux* form of the $y$-momentum equation:

$$\frac{\partial(vd)}{\partial t} + \frac{\partial}{\partial y}\left[v^2 d + gd^2/2\right] = 0\,. \qquad (1.6.11)$$

This result can also be obtained by multiplying (1.2.1) by $d$ and using the continuity equation (1.2.2). Although it is formally invalid within the jump, (1.6.11) yields the correct matching condition when integrated across a discontinuity in depth. Numerical solutions of the shallow water equations based on the finite-difference method (e.g. Helfrich *et al.* 1999) frequently use (1.6.11) in place of (1.2.1) since the resulting solutions better approximate the correct matching conditions when jumps and bores are present.

*c. Entrainment from an overlying layer.*

The above discussion has assumed a single layer flow with a free upper surface, but most ocean and atmospheric applications will involve an overlying or underlying fluid with slightly different density. Experiments by Wilkinson and Wood (1971) reveal the anatomy of such a jump when the second fluid is relatively deep and inactive (Figure 1.6.4). The jump consists of two stages, an upstream region in which overlying fluid is entrained down into the moving layer, and a 'roller' region with a large counterclockwise eddy. The roller region was found to produce relatively little entrainment. The Froude number based on reduced gravity remains <1 in the entrainment region and jumps to below unity downstream of the roller. Entrainment is produced by shear instabilities at the interface between the two fluids. At the top of the roller, where the horizontal velocity is negative and the vertical shear is reduced relative to upstream values, entrainment is not observed. By traditional definition the entrainment region and the roller comprise the hydraulic jump, even though the entraining region may be much longer than the roller.

The presence of entrainment gives rise to a significant departure from the single-layer case considered earlier. One of the consequences is that for a given upstream state there is no unique downstream state. As demonstrated by Wilkinson and Wood, a range of downstream states may be found by varying the height $h_m$ of an obstacle placed downstream of the jump (Figure 1.6.4). Lowering $h_m$ causes the roller region to migrate downstream, lengthening the entraining regions and increasing the total amount of entrainment. For sufficiently small $h_m$ the roller disappears and the jump consists entirely of a gradually deepening region of entrainment. This is the state of maximum entrainment. If $h_m$ is increased, the roller moves upstream and eats up the entrainment region. For sufficiently large $h_m$ the entrainment region disappears and the jump consists only of the roller. A further increase in $h_m$ causes the roller to come into contact with the vertical wall beneath which lower layer fluid is injected. The jump at this point is said to

be flooded. Photographs of the three cases (no roller, combination of entrainment region and roller, and flooded jump) are shown (Figure 1.6.5) for the Wilkinson and Wood experiment, an upside-down version of the scheme we have been discussing.

Entrainment gives rise to a lack of conservation of mass and volume flux in the lower layer. If $E$ is the volume flux per unit width introduced into the lower layer by entrainment, then the mass and volume budgets for the lower layer between sections immediately upstream and downstream of the jump (Figure 1.6.5) are

$$v_u d_u + E = v_d d_d \tag{1.6.12}$$

and

$$\rho_u v_u d_u + E\rho_1 = \rho_d v_d d_d ,$$

where $\rho_1$ is the upper layer density and $\rho_u$ and $\rho_d$ are upstream and downstream values of the lower layer density. Subtraction of the product of $\rho_1$ and the first equation from the second leads to

$$(\rho_u - \rho_1) v_u d_u = (\rho_d - \rho_1) v_d d_d ,$$

which is often written in the form

$$g'_u v_u d_u = g'_d v_d d_d , \tag{1.6.13}$$

where $g'_u = g(\rho_u - \rho_1)/\rho_1$ and similarly for $g'_d$. The quantity $g'vd$ is called *buoyancy flux* and its conservation is a consequence of the total conservation of mass for the two layers as a whole.

Further complicating the problem of shock joining is the fact that a horizontal pressure force, exerted by the overlying fluid, now exists on the upstream face of the roller and the top of the entraining region. However, the flow force for the two layers as a whole remains conserved provided that contributions from the bottom slope and frictional bottom drag are negligible. To find the total flow force, we assume that the upper layer is motionless, implying that the free surface ($z=D$) is level. Integrating the hydrostatic pressure over the whole depth of the layer then leads to

$$g\rho_1 \frac{D^2}{2} + g(\rho_u - \rho_1)\frac{d_u^2}{2} + d_u v_u^2 = g\rho_1 \frac{D^2}{2} + g(\rho_d - \rho_1)\frac{d_d^2}{2} + d_d v_d^2 \tag{1.6.14}$$

The first term on each side of the equation is the barotropic pressure force, equal to the force that would exist if the fluid had uniform density $\rho_1$. The second term is the extra pressure force due to the excess density of the lower layer. Cancel the barotropic terms and one is left with an expression identical in form to the case of a single layer (*cf.* 1.6.3).

If the entrainment $E$ is known, then (1.6.12-1.6.14) provide three relations allowing the downstream velocity, layer depth, and density to be calculated from their upstream values. Of course $E$ is not known in advance nor, as shown by the experiment, can it be predicted solely on the basis of the upstream state. Some sort of downstream information, or an assumption about the downstream flow, must be made. An approach taken by Wilkinson and Wood (1971) is to assume that the downstream flow is hydraulically controlled by an obstacle of height $h_m$, as in the experiment. It is further assumed that no entrainment or dissipation occurs between the downstream section $x_d$ and the sill. Although two additional unknowns (the velocity and layer thickness at the sill) are introduced, there are three constraints. These include conservation of energy and volume flux as well as the critical condition at the sill. For given $h_m$ the entrainment can be calculated and the problem closes.

Although this last procedure is elegant, it is difficult to apply in geophysical settings due to the general lack of a clearly defined downstream obstacle or $h_m$ value. Supercritical flows often spill out onto vast terrestrial or abyssal plains and the factors controlling the downstream layer thickness are complex. Alternatives to the Wilkinson and Wood procedure use turbulence closure assumptions to predict the energy dissipation or entrainment in the jump. The reader is referred to the work by Qinfang and Smith (2001a,b) and Holland *et al*. (2002) and references contained therein.

*d. Form drag.*

We close this section with a brief description of *form drag*, a property that is strongly influenced by the presence and location of a hydraulic jump. Consider a steady, free surface flow over an obstacle in a channel of uniform width (Figure 1.6.6a). Integration of the steady form of the flux form (1.6.11) of the momentum equation (1.6.11) between sections *a* and *b* leads to

$$\left[ v^2 d + g d^2 / 2 \right]_a^b = -\int_a^b \left( g d \frac{dh}{dy} \right) dy \qquad (1.6.17)$$

Thus the difference between the flow force at either end of the obstacle is equal to the integral of the horizontal component of bottom pressure $gd$ over the obstacle. For the hydraulically controlled flow shown in the figure, the pressure on the upstream face of the obstacle is generally greater than on the downstream face and thus the obstacle exerts a net force on the flow in the upstream direction. This type of 'drag' requires no bottom friction or viscosity. If the hydraulic jump lies closer to the sill in the figures, the depth over the downstream part of the obstacle increases and the form drag is reduced. The maximum drag occurs when the jump is absent. When the flow has upstream or downstream symmetry with respect to the topography, such as in a purely subcritical or supercritical state, the form drag is zero.

The concept of form drag is most meaningful when the object in question is isolated. If the topography in the example begins at one elevation $h$=0 but ends at another $h$=$h_o$ (Figure 1.6.6b), then even a resting fluid experiences a form drag as computed by the integral in (1.6.17). This difficulty can be removed by performing the integration between two sections of equal bottom elevation, say $a'$ and $b$ in the figure. However, the resulting form drag is more arbitrary and may or may not be of interest. Geophysical applications typically involve two-dimensional topographic variations, making it even more difficult to define isolated objects. If the channel axis bends substantially, the use of a linear ($y$-) momentum balance itself becomes less meaningful. Edwards *et al.* (2004) describe an example and suggest ways of dealing with some of these complications.

**Exercises**

1) Derive the shock joining conditions for a hydraulic jump in a channel with the same triangular cross-section as that given in problem 4 of Section 1.4. The fluid is homogeneous and has a free surface.

2) Consider a bore propagating in a homogeneous, free-surface flow with spatially and temporally varying velocity and depth. The speed of the bore is unsteady: $c_1$=$c_1(t)$. Define a material volume $V$ bounded by the free surface, the side walls of the channel, and by material fluid columns located at position $a(t)<y<b(t)$ as shown in Figure 1.6.2. Also, let $y_u$ and $y_d$ be fixed positions lying within the volume as shown in the figure.

(a) Show that

$$\frac{d}{dt}\iiint_V v\,dxdydz = w\left[\frac{d}{dt}\int_{a(t)}^{y_u}(dv)dy + \frac{d}{dt}\int_{y_u}^{y_d}(dv)\,dy + \frac{d}{dt}\int_{y_d}^{b(t)}(dv)dy\right]$$

(b) Note that the above equation also applies in a steadily translating frame of reference. Let the speed of translation be $c_1(0)$, so that the frame speed matches the bore speed at $t$=0. By shrinking the distances between $a(t)$, $y_u$, $y_d$, and $b(t)$ to zero , show that at $t$=0

$$\frac{d}{dt}\int_{a(t)}^{y_u}(dv)dy \to -v_u^2 d_u$$

$$\frac{d}{dt}\int_{y_u}^{y_d}(dv)\,dy \to 0$$

$$\frac{d}{dt}\int_{y_d}^{b(t)}(dv)dy \to v_d^2 d_d$$

where $v_u$=$(\,da/dt)_{t=0}$ and $v_d$=$(db/dt)_{t=0}$.

(c) By applying (1.6.10) and evaluating the forcing terms on the right-hand side using the hydrostatic pressure at $y=a(0)$ and $y=b(0)$, show that (1.6.3) is recovered. Note that (1.6.5) follows by transformation back to a rest frame.

(d) Perform the same series of operations starting with a primitive statement of mass conservation in order to recover (1.6.4) for an unsteady shock.

3) Consider two sections $a$ and $b$ of a channel in which the width $w(y)$ and topographic elevation $h(x,y)$ are identical. Between the two sections the topography and width vary. Define a generalized form drag between $a$ and $b$.

4) *Form drag and energy dissipation.* Consider the situation shown in Figure 1.6.6a: a 2D flow over an obstacle with a hydraulic jump in the lee.

(a) Show that the form drag and energy dissipation between the sections $a$ and $b$ can be written in terms of the upstream Froude number and the ratio of downstream to upstream depths as

$$\tilde{D}_f = F_a^2 + \frac{1}{2} - F_a^2\left(\frac{d_b}{d_a}\right)^{-1} - \frac{1}{2}\left(\frac{d_b}{d_a}\right)^2 \qquad (1.6.18)$$

$$\tilde{E} = \frac{1}{2}F_a^2 + 1 - \frac{1}{2}F_a^2\left(\frac{d_b}{d_a}\right)^{-2} - \left(\frac{d_b}{d_a}\right) \qquad (1.6.19)$$

where

$$\tilde{D}_f = \frac{D_f}{g d_a^2} \ , \quad \tilde{E} = \frac{-\dot{E}}{g v_a d_a^2},$$

and where $F_a^{\,2} = \dfrac{v_a^{\,2}}{g d_a}$ is the Froude number based on the upstream state.

(b) Show that the Jacobian $J_{F_u,(d_b/d_a)}(\tilde{E},\tilde{D}_f)$ is nonzero and thus there is no direct functional relation between $\tilde{D}_f$ and $\tilde{E}$.

(c) However, for a fixed $F_u$, we know that the maximum values of $\tilde{D}_f$ and $\tilde{E}$ occur when the hydraulic jump lies right at the foot of the obstacle. As the jump is moved towards the sill and its amplitude decreases, so do $\tilde{D}_f$ and $\tilde{E}$. Show, in fact, that the maximum value of the Jacobian

$$J_{F_u,(d_b/d_a)}(\tilde{E},\tilde{D}_f)$$

is numerically small (<0.05) over the permissible range of $F_a$ and $d_b/d_a$. (Note that $0 \le F_a \le 1$ and for each $F_a$ there is a range $(d_b/d_a)_{min} \le d_b/d_a \le 1$ corresponding to various positions of the hydraulic jump. This range varies from the sill, for which $d_b/d_a=1$ and the foot of the obstacle, for which $d_b/d_a$ has a minimum value.) Thus $\tilde{E}$ may be considered a function of

$\tilde{D}_f$ to a first approximation. In fact, Ms. Christie Wood has shown that $\tilde{E} = 0.9744\tilde{D}_f + 0.8608\tilde{D}_f^2$ with in an error of ????.

**Figure Captions**

1.6.1 Schematic depiction of the various types of shallow-water adjustment caused when an obstacle is introduced into a uniform, subcritical stream (a). In (b) the obstacle height is less than the critical value and the flow remains subcritical. In (c) the obstacle exceeds its critical height and a hydraulically controlled flow with a jump emerges. In such cases the jump may also propagate downstream as a bore. In (d) the obstacle has exceeded the height required for complete blocking. (The downstream disturbances are not shown for this case.)

1.6.2 An abstraction of a hydraulic jump.

1.6.3 The foamy wave front is a bore, formed by the leading edge of a wave propagating onto a gently sloping beach in southern California. The wavy feature to the right is an undular bore that is propagating in the opposite direction (right-to-left). The latter is formed at the leading edge of a long wave that has been reflected from the beach. (L. Pratt photo.)

1.6.4. A schematic view of the two-fluid jump observed by Wilkinson and Wood (1971).

1.6.5 Photographs of the laboratory experiment of Wilkinson and Woods (1971).

1.6.6 (a) The horizontal distribution of bottom pressure leading to form drag. The arrows show the normal and horizontal components of bottom pressure *gd* at two points of equal elevation. The resisting pressure force on the upstream face of the obstacle exceeds the enhancing force on the downstream face. (b) If the obstacle is not isolated, it will exert an net horizontal pressure force even if the fluid is at rest. This effect can be removed by relocating the upstream and downstream sections to lie at equal elevation, as indicated by $a'$ and $b$.

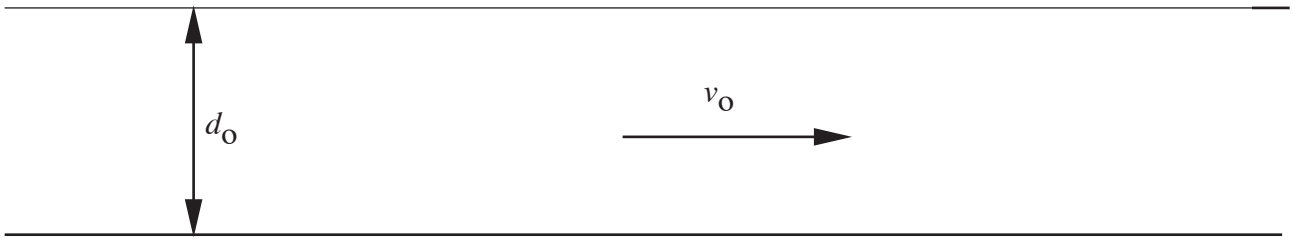


(a) initial flow

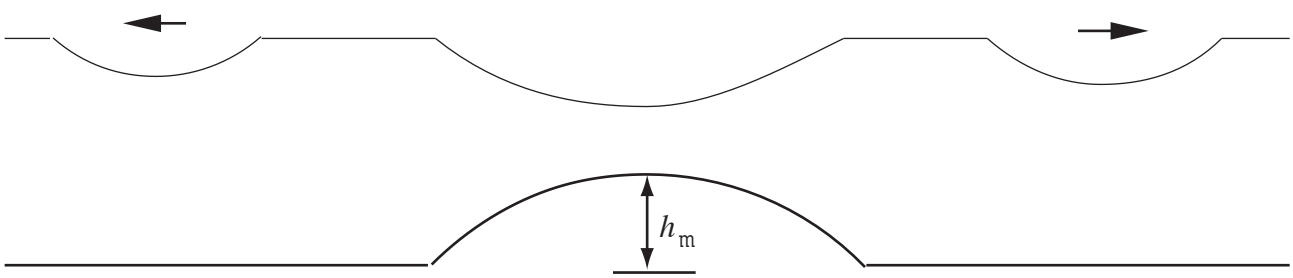


(b) no blockage ($F_0 < 1$)

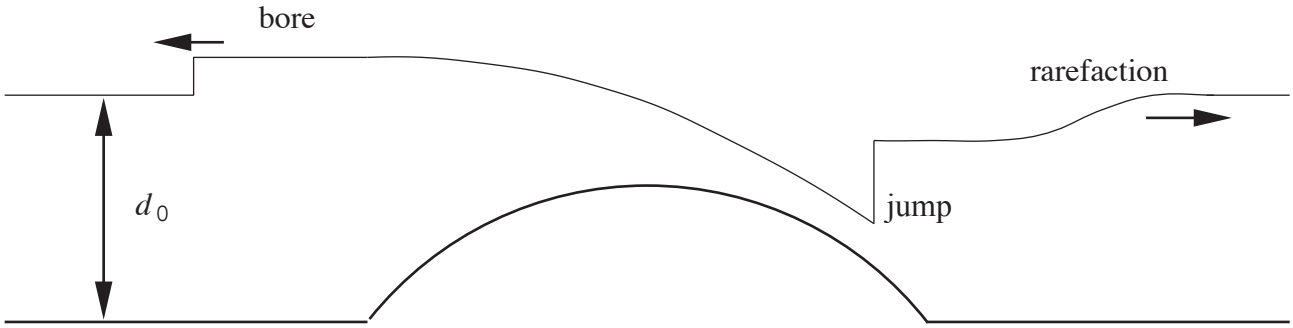


(c) partial blockage

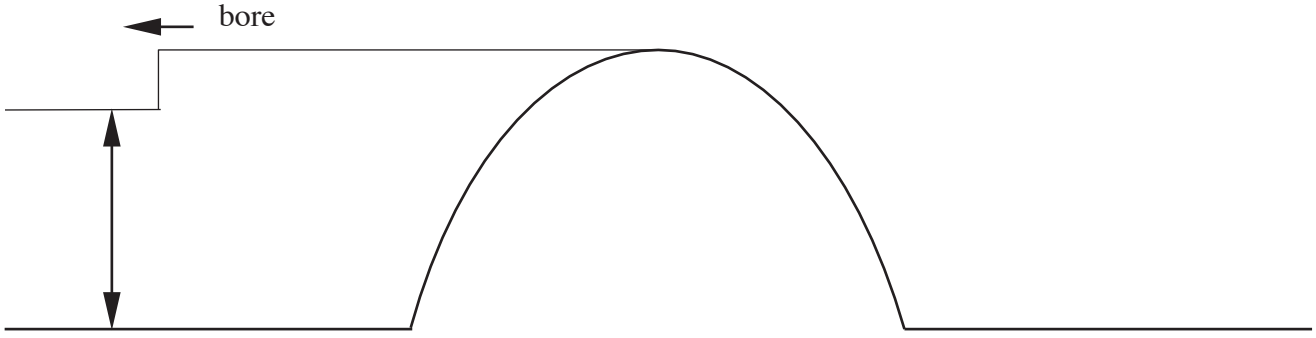


(d) total blockage

Figure 1.6.1

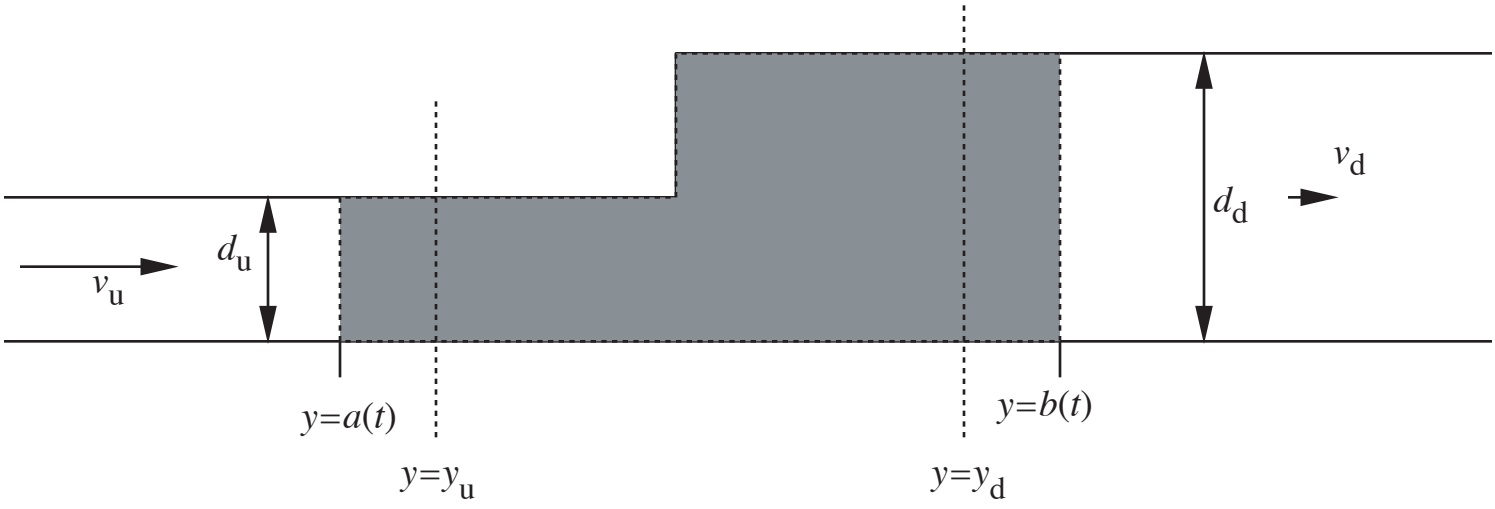


Figure 1.6.2

Figure 1.6.3

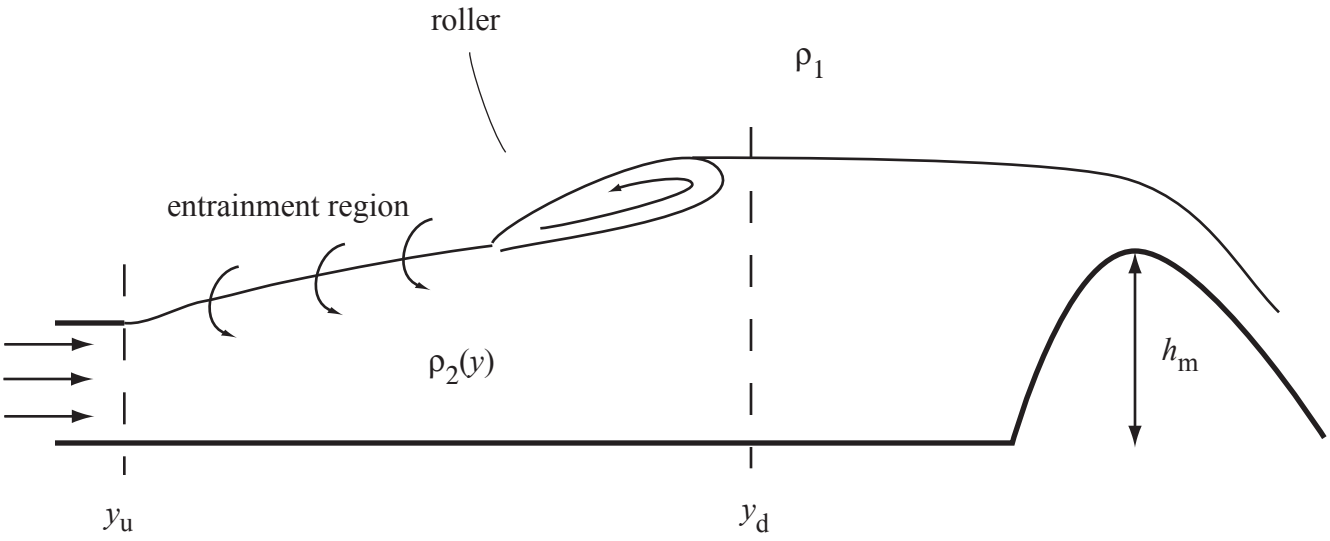


Figure 1.6.4

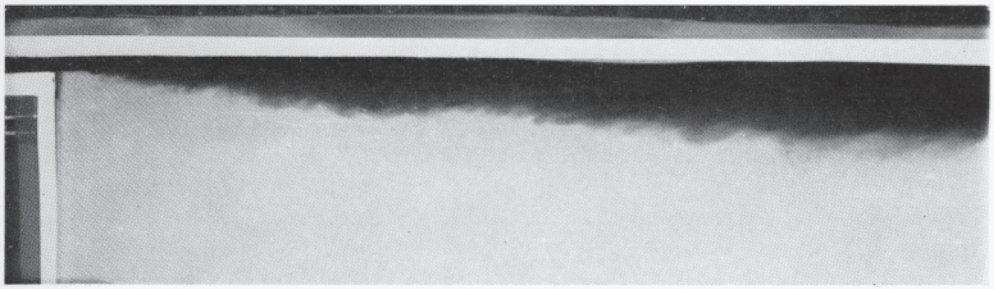

A density jump of the maximum entraining type with a free overfall downstream. Entrainment is occurring along the length of the jump.

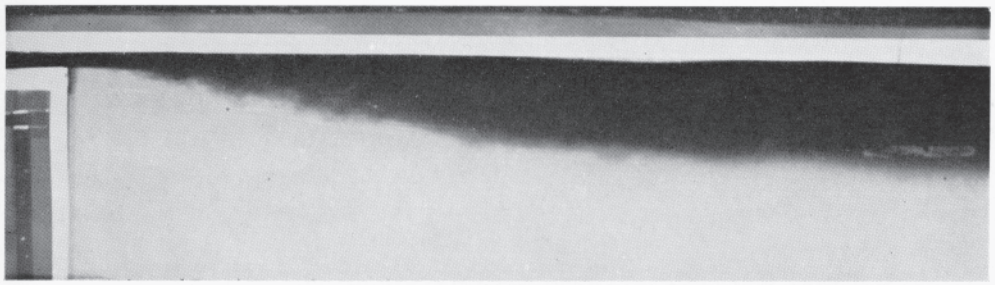

. A density jump controlled by a broad crested weir downstream. Entrainment is occurring only at the far upstream end of the jump, the remainder consists of a roller zone.

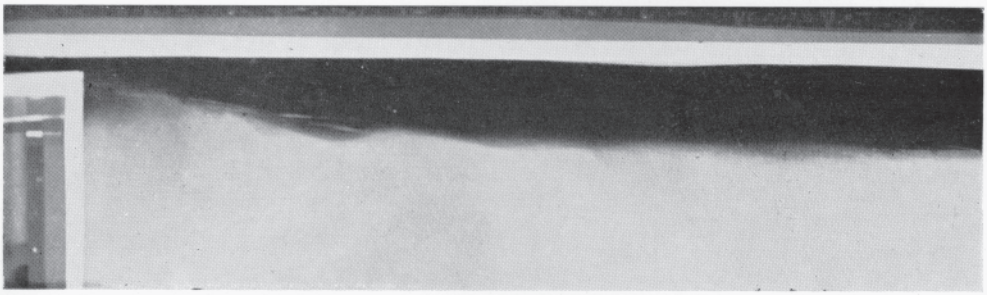

Photograph of a flooded density jump. The inlet flow for this jump is identical to that of the jumps shown in figures 1 and 2.

Figure 1.6.5

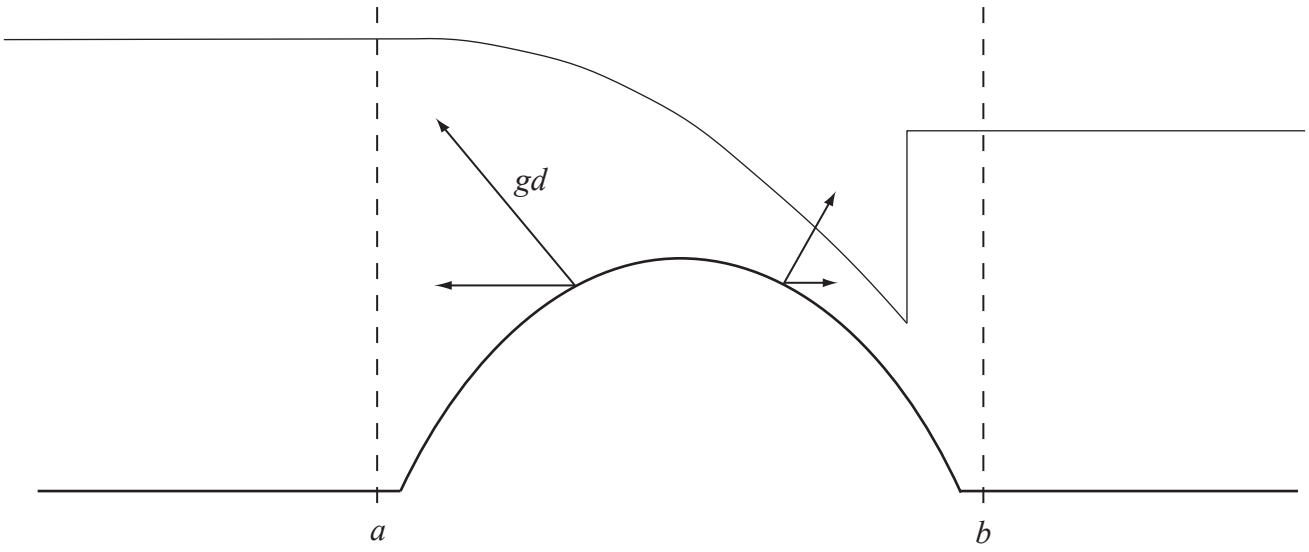


(a)

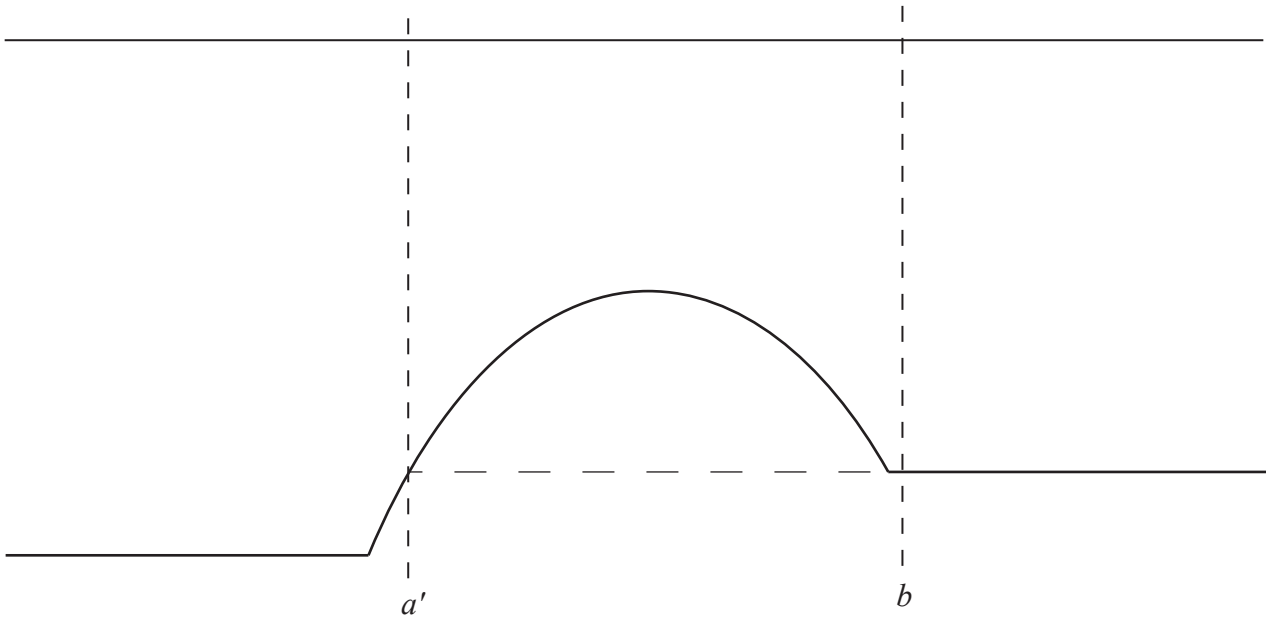


(b)

Figure 1.6.6